Nanoscale characterization of β-phase $H_xLi_{1-x}NbO_3$ layers by piezoresponse force microscopy

Michele Manzo,[1] Denise Denning,[2] Brian J. Rodriguez,[2] and Katia Gallo[1]
[1]*KTH—Royal Institute of Technology, Department of Applied Physics, 106 91 Stockholm, Sweden*
[2]*University College Dublin, School of Physics, Belfield, Dublin 4, Ireland*

(Received 11 February 2014; accepted 18 April 2014; published online 11 August 2014)

We investigate a non-destructive approach for the characterization of proton exchanged layers in $LiNbO_3$ with sub-micrometric resolution by means of piezoresponse force microscopy (PFM). Through systematic analyses, we identify a clear correlation between optical measurements on the extraordinary refractive index and PFM measurements on the piezoelectric d_{33} coefficient. Furthermore, we quantify the reduction of the latter induced by proton exchange as $83 \pm 2\%$ and $68 \pm 3\%$ of the $LiNbO_3$ value, for undoped and 5 mol. % MgO-doped substrates, respectively.
 [http://dx.doi.org/10.1063/1.4891352]

I. INTRODUCTION

Due to its high piezoelectric, electro-optic, pyroelectric, photovoltaic and nonlinear optical coefficients, lithium niobate (LN) is a material of technological relevance for a variety of applications, ranging from surface acoustic wave filters,[1] pyroelectric detectors,[2] high speed modulators,[3] and laser frequency converters,[4] to templates for ferroelectric lithography and artificial photosynthesis.[5,6] All of the above properties are (directly or indirectly)[7] related to the elevated spontaneous polarization ($\sim 75\ \mu C/cm^2$) of the material, which can be patterned by electric field poling and chemical techniques.[4,8]

Proton exchange (PE) is a process relying on the controlled introduction of protons in LN via a thermally activated ion-exchange ($H^+ \leftrightarrow Li^+$).[9] It was originally devised for integrated optics,[10] but it also opens up possibilities for domain engineering and ferroelectric lithography on LN substrates.[5,8,11,12] Conventional characterizations of PE in LN, made by optical techniques[13,14] are inherently limited in their spatial resolutions by beam cross-sections (in the micrometric range), while alternative methods, which can enable nanoscale imaging, are often cumbersome and destructive.[15,16] On the other hand, as LN technology is pushed to the nanoscale in 3D device engineering,[5,17] non-destructive and high-resolution characterizations of the material properties become essential.

Piezoresponse force microscopy (PFM) is nowadays widely used for nanoscale imaging of ferroelectric domains.[18,19] Furthermore, it can enable 3D reconstruction of the spontaneous polarization by combining vertical and lateral PFM,[20] estimation of piezoelectric coefficients,[21] and nanoscale characterization of ferroic samples with proton in-diffusion.[16,22]

In this work, we present a coherent study on selectively proton-exchanged LN substrates, demonstrating the viability of a PFM approach for non-destructive high-resolution imaging of the PE regions. The PFM results obtained for congruent LN crystals are consistent with the expected impact of protons on the spontaneous polarization[12,23] and provide experimental evidence for a correlation between optical properties and spontaneous polarization at sub-micrometric scales.[7,24] The data are used for a quantitative evaluation of the impact of PE on the piezoelectric properties (d_{33} coefficient) of LN, with and without MgO-doping. The latter substrates are attracting a growing interest in both traditional and emerging applications of $LiNbO_3$, i.e., in nonlinear integrated optics and ferroelectric lithography.[25,26]

II. EXPERIMENTAL

The experiments were conducted on commercially available *z*-cut LN substrates (undoped and 5 mol. % MgO-doped LN wafers from CasTech Inc. and Roditi Ltd., respectively), which were selectively proton-exchanged in pure benzoic acid at 200 °C for 24 h. This resulted in $\sim 3\ \mu$m-thick $H_xLi_{1-x}NbO_3$ ($\sim 2\ \mu$m-thick MgO:$H_xLi_{1-x}NbO_3$) layers, as estimated from optical measurements. To define the PE patterns, we used periodic Ti masks ($\Lambda = 6.09\ \mu$m, ~50% duty cycle), fabricated by reactive ion etching (Cl_2-Ar RIE). The mask was finally removed after PE by wet etching (a few seconds in a 48% HF:H_2O solution). Fig. 1(a) illustrates the final structure of the samples, containing PE stripes on the *z*-surface, periodic along the *x* direction and parallel to the *y* crystallographic axis, of width w_{PE} and maximum depth d_{PE} (along *x* and *z*, respectively).

The PE process implies an increase of the extraordinary refractive index (Δn_e) with respect to the bulk crystal, suitable for the formation of surface optical waveguides. The depths (d_{PEz}) resulting from our fabrication conditions sustained several guided modes (TM polarized, given the substrate polarity). This allowed evaluating the depth profile of the refractive index increase, $\Delta n_e(z)$, by means of waveguide optical m-line spectroscopy techniques,[27] based on measurements of the effective indices of the guided modes and reconstruction of the index profile by inverse Wentzel-Kramers-Brillouin (IWKB) algorithms.[13,28] Fig. 1(b) shows the depth evolution of the extraordinary refractive index increase across the PE layer for LN (solid) and 5 mol. % MgO-LN (dashed line) as inferred from such optical characterizations. The data of Fig. 1(b) show a step-index profile, and a surface refractive index increment (Δn_e at $z = 0$) higher

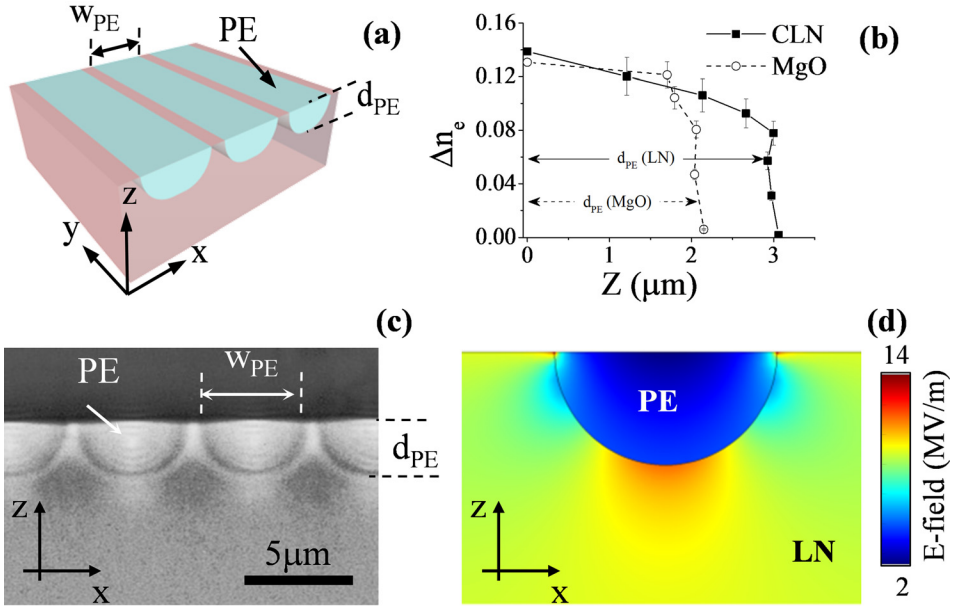

FIG. 1. (a) 3D sketch of the sample geometry used for the PFM measurements, consisting of periodic proton-exchanged stripes (PE) on a *z*-cut LN substrate, of width w_{PE} (along *x*), and depth d_{PE} (along *z*). (b) Profile of the extraordinary refractive index increase (Δn_e) as a function of depth (*z*) obtained as result of m-line spectroscopy and IWKB reconstruction for planar PE in LN samples with (circles) and without (squares) 5 mol. % MgO doping. (c) Cross-sectional view of end-face polished PE stripes (*x*-*z* plane). The image is obtained in transmission with an optical microscope. (d) Spatial distribution of the electrostatic field in the *x*-*z* plane by the PE:LN interface, calculated (attributing $P_s = 0$ to the PE region) with COMSOL Multiphysics 4.3.

than 0.13 for both 5 mol. % MgO-doped and congruent LN. In light of the existing structural phase diagrams for $H_xLi_{1-x}NbO_3$ on *z*-cut undoped LN substrates,[23,29] the observed index increase appears typical of surface β-phase $H_xLi_{1-x}NbO_3$ layers (specifically β_3 surface layer with a β_1 sublayer),[30] which features the $Li^+ \leftrightarrow H^+$ exchange ratios $x > 0.5$ and an abrupt phase-boundary with LN.[31] From Fig. 1(b), the 1/e PE-depths were estimated to be: $d_{PE} \sim 2.97\ \mu m$ for LN and $d_{PE} \sim 2.04\ \mu m$ for MgO:LN.

Fig. 1(c) is a cross-sectional view of the periodic PE stripes in LN samples. The PE regions appear brighter, as the increase of the refractive index (Δn_e) confines more light therein. From the image, one can estimate $d_{PE} \sim 3\ \mu m$ and $w_{PE} \sim 5\ \mu m$ (for PE with 1.3 μm-wide Ti mask openings). Additional contrast in the optical image can be attributed to the presence of electrical fields at the PE:LN boundary, which affect the local refractive index via the electro-optic effect.[24] This is qualitatively illustrated by Fig. 1(d) where we plot the calculated *x*-*z* distribution of the electrostatic field arising from the discontinuity of the spontaneous polarization (P_s) at the PE:LN boundary.[8] The contrast in Fig. 1(c) maps with good fidelity the E-field intensity pattern of Fig. 1(d).

β-phase PE layers exhibit a pronounced degradation of the ferroelectric properties of LN,[31] as the protons substituting for the Li^+ ions place themselves in a shifted position along the *z*-axis, substantially reducing the spontaneous polarization.[32] Such a difference results in a contrast in the d_{33} piezoelectric coefficient, which can be retrieved by vertical PFM measurements on *z*-cut substrates,[18,19] to afford local and non-destructive visualizations of PE areas.

By applying a classical thermodynamic approach to the case of $LiNbO_3$ (a ferroelectric with a second order phase transition and a centrosymmetric paraelectric phase),[33] a law of direct proportionality between the d_{33} coefficient and P_s can be inferred. Following the derivations of, e.g., Ref. 33 for the one-dimensional case (polarization and applied E-field along *z*), one obtains:

$$d_{33} = 2\varepsilon_{33} Q P_s, \tag{1}$$

ε_{33} and *Q* being the dielectric constant and the electrostrictive coefficient relative to the *z*-axis. The vertical PFM response ($\propto d_{33}$) in *z*-cut substrates such as those of Fig. 1 is therefore bound to provide insights on the local impact of protons on the ferroelectric properties of LN.[18,22]

The PFM experiments were performed on the *x*-*y* plane, with the sample geometry of Fig. 1. The cantilever was aligned to *y* and moved along *x*, so to comprise both PE and LN regions in a single scan. We sampled scanning speeds between 10 and 60 μm/s without seeing significant differences in the response, hence we illustrate the results for only one of them ($v_{sc} = 22.5\ \mu m/s$). We used doped silicon cantilevers (PPP-NCH Nanosensors, nominal spring constant, resonant frequency and radius of curvature of: 42 N/m, 330 kHz, and 50 nm, respectively). The AC voltage (V_{AC}) was applied through the tip, predominantly along the *z*-axis of the substrate, while grounding the counter electrode. To sample the d_{33} coefficient, the vertical PFM signal (S_z) was extracted as the first harmonic component of the cantilever oscillations (amplitude, $|S_z|$, and phase, Φ, of the out-of-plane response).

The cantilever motion results from a superposition of electromechanical, electrostatic, and non-local interactions at the sample surface:[34,35]

$$S_z = A_{EM} + A_{ES} + A_{NL}. \tag{2}$$

The electromechanical response is determined by the converse piezoelectric effect and in our configuration maps d_{33}, i.e., $A_{EM} = d_{33} V_{AC}$. Non-local interactions (A_{NL}) can be minimized by the use of stiff cantilevers and tips with high aspect-ratios and usually contribute as an offset.[36] The electrostatic component induces a Maxwell force ($F_{AC} = -V_o V_{AC}\, dC/dz$, V_o being the DC voltage at the tip-sample interface),[34] which also affects the demodulated PFM signal S_z at the fundamental frequency ν_{AC}. We account for all such effects (in a linear regime) through an offset (S_0) and a multiplicative factor (α) in the PFM response, i.e.,

$$S_z = S_o + \alpha d_{33} V_{AC}, \quad (3)$$

and α is an empirical constant dependent on several parameters (e.g., nature of tip and substrate, tip indentation, humidity, operational frequency, etc.),[37] not necessarily reproducible from one measurement to another, which generally hampers the retrieval of *absolute* values of d_{33}.[37,38] Nevertheless, in our experimental configuration (Fig. 1) contiguous PE and LN stripes are sampled in a single scan, under identical conditions, and one can reasonably assume S_o and α to remain the same. This, as discussed later, enables reliable *relative* measurements of the d_{33} in PE with LN as a reference.

III. RESULTS AND DISCUSSION

A. PE imaging

Fig. 2 exemplifies the PFM imaging capabilities on PE:LN, by showing both topographic [height, Fig. 2(a)] and piezoelectric [mixed signal: $|S_z|\cos(\Phi)$, Fig. 2(b)] responses recorded on the sample of Fig. 1. The data are also shown as 1D scans in Fig. 2(c). The scans are made along the very same line [highlighted in Figs. 2(a) and 2(b)]. Red (black) markers correspond to the topographic (PFM) signal.

The topography image [Fig. 2(a)] allows a clear visualization of periodic stripes of the crystal (where the original PE mask openings were located), which were over-etched in the RIE process during the mask fabrication. Such RIE-PE areas are depressed [Fig. 2(c), red trace], appear darker and have circular protrusions [cf also high-resolution image, Fig. 2(d)].

During PE, protons diffused into the crystal from the Ti-mask openings, in depth (z) but also laterally (along x, i.e., under the mask), creating lateral diffusion (LD) stripes to the sides of the original RIE tracks. This is apparent from a comparison between Fig. 2(a) (RIE tracks) and the PFM map of Fig. 2(b). The latter highlights a strong contrast between virgin LN and PE regions (RIE + LD areas), which appear as dark stripes on a brighter (LN) background, consistently with the expected reduced piezoelectric response of PE areas.

The PFM mixed signal [Fig. 2(b)] also contains information on the phase of the piezoresponse, reflecting the substrate polarity,[39] which is left unchanged by PE (i.e., $\Phi_{PE} \sim \Phi_{LN}$). Accordingly, the contrast of Fig. 2(b) essentially maps changes in the amplitude of the piezoresponse from PE (S_{PE}) and LN (S_{LN}) regions. The amplitude of the PFM signal [black circles, Fig. 2(c)] abruptly drops upon crossing the boundary of the PE regions, which is also in good agreement with the sharp crystallographic phase-front expected at the interface between $LiNbO_3$ and β-phase PE.[10] Such well-defined transitions allow a precise evaluation of the spatial extent of PE ($w_{PE} = 4.74\ \mu$m), with much better accuracy than optical tools.

No contribution to the PFM signal of local charging in the ion-etched areas is apparent from the data of Figs. 2(a)–2(c). Furthermore, the profiles in Fig. 2(c) indicate the absence of significant crosstalk between the topographic (RIE etching) and the PFM (PE) signals. This was achieved by a careful tuning of the optimal parameters for PFM imaging, in particular of the frequency, ν_{AC}, which was chosen to be far from contact resonances (to reduce any frequency-dependent cross-talk).[40] Further details on the procedures adopted to ensure consistency and reproducibility of the PFM measurements are discussed in Sec. III B.

The results illustrated by Fig. 2 were further confirmed by similar PFM mappings made on samples with various PE

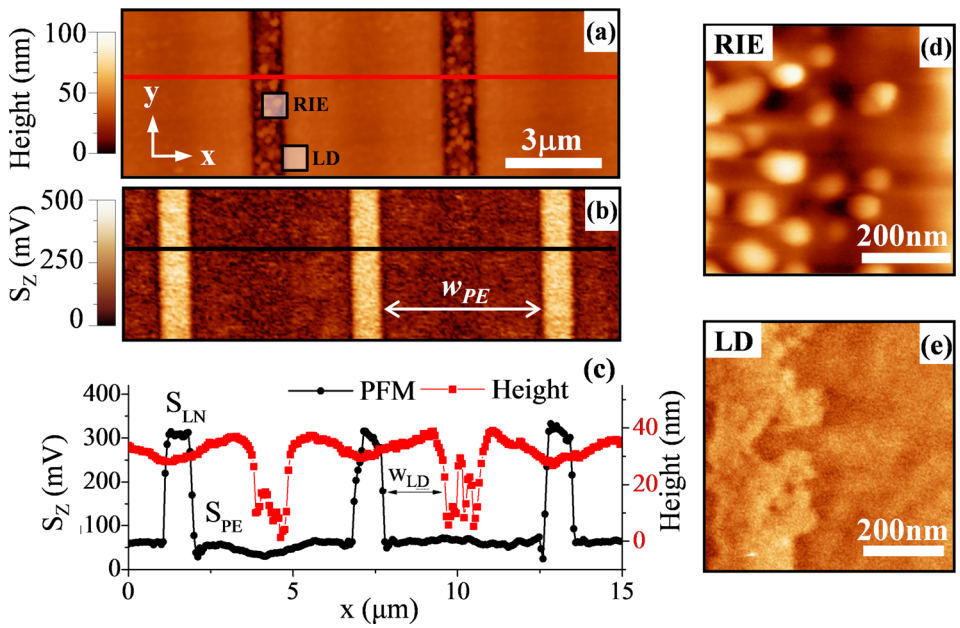

FIG. 2. PFM measurements obtained from PE:LN samples of the kind shown in Fig. 1 ($t_{PE} = 24$ h at 200 °C, $d_{PE} \sim 3\ \mu$m). (a) Topography of the sample with the over-etched RIE regions appearing as narrow stripes aligned along y. (b) 2D map of the piezoresponse (mixed signal) recorded in the same location of (a) (imaging conditions: $V_{AC} = 5$ V, frequency $\nu_{AC} \sim 1.5$ MHz, scanning speed $v_{sc} = 22.5\ \mu$m/s); the dark (bright) areas are PE (non-PE) regions. (c) Line profiles extracted at the same location for topography [(a), red] and PFM [(b), black] scans. The topography shows the depth (~ 35 nm) and the width ($\sim 1.3\ \mu$m) of the openings for PE fabricated by means of RIE; in the PFM signal S_{LN} corresponds to the bare crystal and S_{PE} to PE regions. (d),(e) High resolution topographical images of the surface status within the PE region: the *RIE* and surface lateral diffusion region, *LD*, are imaged at the locations framed in (a).

depths ($d_{PE} \in [0.5, 8]$ μm, adjusted by controlling the exposure time to benzoic acid), on both $+z$ and $-z$ surfaces, demonstrating the possibility to readily visualize β-phase PE regions with nanoscale resolutions, without resorting to any etching. A good agreement was consistently found between optical (n_e) and PFM (d_{33}) results, providing evidence for a direct link between the local increase of the extraordinary refractive index and the decrease of the spontaneous polarization in PE layers ($\Delta n_e \propto -\Delta P_s$), as originally suggested in Ref. 24.

Scanning probe microscopy tools can also provide further insights into additional features of PE at the nanoscale, for instance, shedding light on questions regarding a possible amorphization of LN as a consequence of PE. According to investigations by X-ray diffraction and/or optical measurements on "macroscopic" PE layers, crystallinity should be preserved in $H_xLi_{1-x}NbO_3$ (although with quite complicated phase diagrams). Yet, this might not be always the case in (shallow) interfacial layers on sub-micrometric scales.[14] We do not have conclusive measurements in this respect, but wish to underline some peculiar features consistently observed, at specific locations on PE surfaces, in high-resolutions topographic images [in Figs. 2(d)–2(e)].

The RIE-PE trenches [Fig. 2(d)] show a very coarse surface with small features (radius < 25 nm), which are likely to originate from material re-deposition, defects and/or ion implantation during the anisotropic etching in Cl_2-Ar atmosphere. In Fig. 2(e), we show instead a portion of the LD PE region, where a highly irregular border, parallel to the PE-RIE windows, is apparent. The leftmost area is closer to a RIE region (i.e., the PE windows) and is slightly (~ 4 nm) higher. The surface swelling would suggest a higher strain in this PE region as compared to the rightmost one. Although not apparent from Fig. 2(b) nor 2(c), such a transition is actually detected as a slight lowering in the PFM response and might well correspond to the boundary between the two $H_xLi_{1-x}NbO_3$ β sub-phases (β_3 and β_1),[10,29] expected to be present within the PE layer [cf. discussion of Fig. 1(b)], although optical characterizations would not allow the location of such boundary to be identified unequivocally.

B. Evaluation of d_{33} reduction in PE

Before proceeding to quantitative assessments of the d_{33} reduction on selectively proton-exchanged undoped and MgO-doped substrates, we first carried out a systematic study to evaluate the reproducibility of the PFM results, since we observed a noticeable dependence of the measurement outcomes on the tip and sample cleaning procedure, as well as on the AC modulation frequency, ν_{AC}, (tunable in the kHz to MHz range).

Our final protocol for the PFM scans included using heavily doped silicon cantilevers (PPP-NCH, Nanosensors) and ozone-cleaning for 20 min before each measurement. As for the choice of ν_{AC}, besides being far from contact resonances to avoid topography leakages into the PFM signal, based on the physical condition that the substrate polarity is unchanged upon PE, we identified the optimal value which corresponded to achieving a difference between the phase response from the PE and the non-PE regions lower than 10% or, in other words, $\Delta\Phi = |\Phi_{PE} - \Phi_{LN}| < 0.1\pi$ in each PFM measurement. Accordingly, for the measurements presented here, optimum values were found to lie around $\nu_{AC} > 1.5$ and 1.8 MHz for LN and MgO-doped LN, respectively (yielding $\Delta\Phi < 0.1\pi$ in both cases). After these calibrations, we proceeded to conduct a systematic analysis of the PE layers on the surfaces of undoped and 5 mol. % MgO-doped LN crystals to extract quantitative information on the d_{33} reduction due to PE.

To extrapolate the *differential* reduction of d_{33} induced by PE versus virgin LN, for undoped and 5 mol. % MgO-doped substrates, we performed multiple PFM scans [as in Fig. 2(b)] on periodically exchanged samples (Fig. 1), by disabling the slow axis scan and progressively varying the AC voltage from 1 to 10 V (in steps of 1 V). An example of such a measurements is shown for undoped LN in Fig. 3(a) (PFM amplitude signal) and Fig. 3(b) (phase). From the latter, one can notice that the piezoresponse of the pure LN crystal [horizontal bright regions in Fig. 3(a)] increases as V_{AC} is raised, whereas the phase [in Fig. 3(b)] does not show appreciable variations, therefore fulfilling the phase criterion ($\Delta\Phi < 0.1\pi$), except for very low V_{AC} values for which the out-of-plane deformation is too low to extract any meaningful phase signal above the noise floor.

From each value of the applied V_{AC}, we retrieved the evolution of the average PFM amplitude in LN ($\bar{S}_{LN}$) and PE areas ($\bar{S}_{LD}$ in LD-PE and $\bar{S}_{RIE}$ in RIE-PE). The results are shown in Figs. 3(c) and 3(d) for PE (24 h, 200 °C) in undoped and MgO-doped LN, respectively. For each sample, the PE data from LD and RIE regions essentially coincide, so we shall just concentrate on the differences between PE and un-exchanged areas.

For both LN and PE areas, in undoped [Fig. 3(c)] and doped [Fig. 3(d)] substrates, the amplitude of the PFM signal grows linearly with the applied voltage (V_{AC}), confirming the validity of Eq. (3) and the reliability of the PFM approach in our experimental conditions. A deviation is only observed for PE regions in MgO-doped LN at voltages greater than 7 V.

Given Eq. (1), the piezoelectric coefficient is related to the slope of the linear fits (solid lines) on the data of Fig. 3. The lower slope of the PE data with respect to LN is a clear indication of the degradation of the piezoelectric properties. From the slopes, one can obtain quantitative assessments of the reduction of d_{33} in PE relative to LN, determined as follows:

$$R = \frac{d_{33}^{LN} - d_{33}^{PE}}{d_{33}^{LN}} = \left.\frac{\partial \bar{S}_{LN}/\partial V_{AC} - \partial \bar{S}_{PE}/\partial V_{AC}}{\partial \bar{S}_{LN}/\partial V_{AC}}\right|_{PFM\ meas} \quad (4)$$

under the assumption that α (in Eq. (3)) is constant in each set of measurements (sample). From the data on Fig. 3, one then obtains: $R_{LN} = 83\% \pm 2\%$ for PE in undoped LN and $R_{MgO} = 68\% \pm 3\%$ for PE in 5 mol. % MgO-doped LN. The reduction of d_{33} is compatible with estimates for the reduction in the spontaneous polarization ($> 80\%$) for comparable β-phase PE waveguides in congruent LN obtainable from, e.g., nonlinear optical measurements.[7,41] On the other hand,

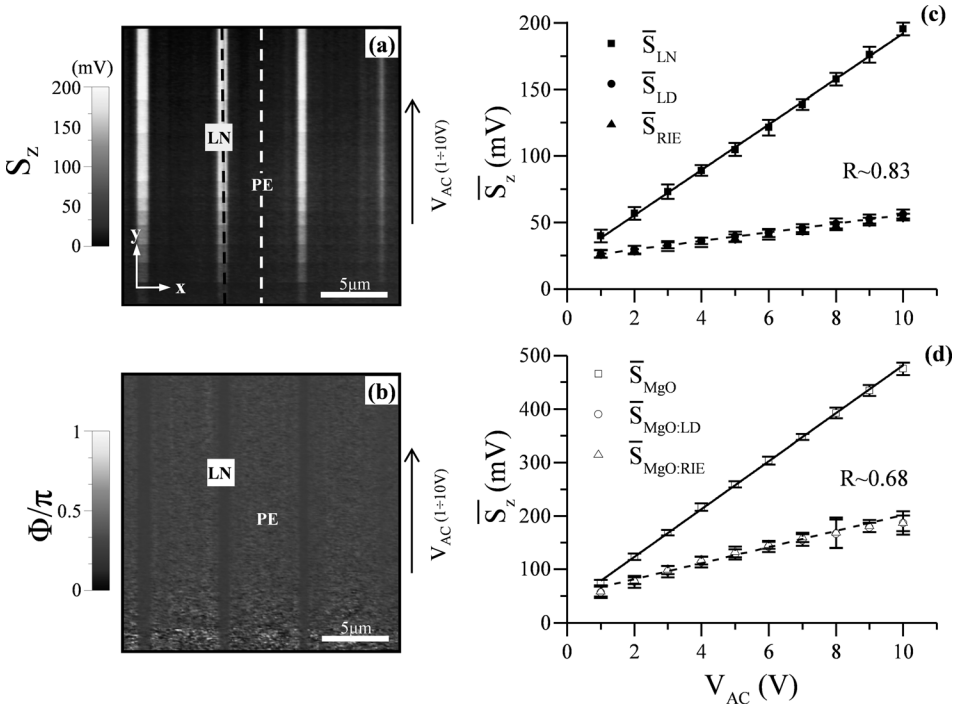

FIG. 3. PFM (a) amplitude and (b) phase 2D images used to quantify the d_{33} coefficient reduction due to PE. The scans were obtained by disabling the slow axis scan (y) and progressively raising the AC voltage (V_{AC}) from 1 to 10 V by steps of 1 V. In (c) and (d) averaged piezoresponse for PE (LD and RIE) and LN regions are plotted as a function of the amplitude of the V_{AC}. Experimental data are shown as markers and linear fits as solid and dashed lines. (c) Congruent LN data for: virgin crystal (squares), lateral diffusion PE-LD (circles) and PE-RIE (triangles) regions ($t_{PE} = 24$ h, $d_{PE} \sim 3$ μm, $\nu_{AC} = 1.6$ MHz, $v_{sc} = 22.5$ μm/s). Extrapolated d_{33} reduction from the linear fits: $R \sim 83\%$. (d) Same as (c) for 5 mol. % MgO-doped LN ($t_{PE} = 24$ h, $d_{PE} \sim 2$ μm $\nu_{AC} = 1.78$ MHz, $v_{sc} = 22.5$ μm/s), yielding: $R \sim 68\%$.

no such estimates are available from the literature for PE in 5 mol. % MgO-doped LN, and at this point we cannot conclusively state whether the observed difference between undoped and MgO-doped substrates is to be simply attributed to a less disruptive impact of PE on the ferroelectric properties of MgO-LN (known to exhibit lower proton incorporation rates),[26,42] or to an enhanced ionic response and possibly capacitive effects associated to the MgO-doping (resulting in different values of S_0 and α in Eq. (3) for LN and MgO-LN). The latter hypothesis might also justify the noticeably higher values of S_z and of the shift at zero voltage (S_o, i.e., the intercept of the linear data fits with the y-axis in Fig. 3) observed in MgO-doped LN ($S_o \sim 50$ mV in MgO-LN to be compared with $\sim$25 mV in LN). Furthermore, the saturation effect observed in the PE-MgO:LN data of Fig. 3(d) above 7 V is a probable indication of the onset of phenomena not included in the model of Eqs. (2) and (3), such as surface electrochemistry and/or ionic motion, which are currently under investigation.

IV. CONCLUSIONS

In conclusion, we implemented a PFM approach for nanoscale non-destructive characterizations of proton-exchanged regions in $LiNbO_3$. We verified its reliability for imaging purposes, by coupling systematic PFM analyses and optical characterizations of β-phases PE regions on $\pm z$-surfaces, in crystals with and without MgO-doping. Furthermore, we applied the PFM method to quantify the reduction of the piezoelectric d_{33} coefficient induced by PE, estimating it to amount to 83% and 68% for undoped and MgO-doped LN crystals, respectively. The proposed method not only provides a practical means to probe the *local* piezoelectric and ferroelectric [Eq. (1)] properties of PE integrated devices but also opens routes to gain further insights into optical and crystallographic properties at sub-micrometric scales (not accessible otherwise). This work addressed correlations between the piezoresponse and linear optical properties (refractive indices). In oxygen octahedra ferroelectrics (such as LN), the electro-optic and nonlinear optical coefficients are also directly proportional to the spontaneous polarization,[7] hence applications of the above PFM technique to, e.g., resolve controversial questions on the optical nonlinearity and phase diagrams,[10] in PE waveguide structures can also be envisaged.

ACKNOWLEDGMENTS

The work was performed in the framework of the COST action MP0702 (STSM 8171), with additional support from Science Foundation Ireland (10/RFP/MTR2855), the Swedish Research Council (VR 622-2010-526 and 621-2011-4040) and the ADOPT Linnaeus Centre for Advanced Optics and Photonics in Stockholm. The authors gratefully acknowledge Liam Collins for technical assistance. The AFM used for this work was funded by Science Foundation Ireland (SFI07/IN1/B931).

K.G. and M.M. dedicate this work to the memory of *Docent* Mårten Stjernström.

[1]C. C. W. Ruppel, L. M. Reindl, and R. Weigel, IEEE Microwave Mag. **3**, 65–71 (2002).
[2]J. H. Lehman, A. M. Radojevic, R. M. Osgood, M. Levy, and C. N. Pannell, Opt. Lett. **25**, 1657–1659 (2000).
[3]E. L. Wooten, K. M. Kissa, A. Yi-Yan, E. J. Murphy, D. A. Lafaw, P. F. Hallemeier, D. Maack, D. V. Attanasio, D. J. Fritz, G. J. McBrien, and D. E. Bossi, IEEE J. Sel. Top. Quantum Electron. **6**, 69 (2000).
[4]M. Yamada, N. Nada, M. Saitoh, and K. Watanabe, Appl. Phys. Lett. **62**, 435 (1993).
[5]N. C. Carville, M. Manzo, S. Damm, M. Castiella, L. Collins, D. Denning, S. A. L. Weber, K. Gallo, J. H. Rice, and B. J. Rodriguez, ACS Nano **6**, 7373 (2012).
[6]M. Stock and S. Dunn, IEEE Trans. Ultrason. Ferroelectr. Freq. Control **58**, 1988 (2011).
[7]M. Di Domenico, J. Appl. Phys. **40**(2), 720 (1969).
[8]M. Manzo, F. Laurell, V. Pasiskevicius, and K. Gallo, Appl. Phys. Lett. **98**, 122910 (2011).

[9]J. L. Jackel, C. E. Rice, and J. J. Veselka, Appl. Phys. Lett. **41**, 607 (1982).
[10]Y. N. Korkishko and V. A. Fedorov, *Ion Exchange in Single Crystals for Integrated Optics and Optoelectronics* (Cambridge Intl Sci. Publ., Cambridge, 1999).
[11]C. Langrock, S. Kumar, J. E. McGeehan, A. E. Willner, and M. M. Fejer, J. Lightwave Technol. **24**, 2579 (2006).
[12]S. Tanzilli, A. Martin, F. Kaiser, M. P. De Micheli, O. Alibart, and D. B. Ostrowsky, Laser Photon. Rev. **6**, 115–143 (2012).
[13]P. K. Tien and R. Ulrich, J. Opt. Soc. Am. **60**, 1325 (1970).
[14]M. L. Bortz, L. A. Eyres, and M. M. Fejer, Appl. Phys. Lett. **62**, 2012 (1993).
[15]A. Loni, R. M. De La Rue, J. M. Zavada, and R. G. Wilson, Electron. Lett. **27**, 1245 (1991).
[16]V. Y. A. Shur, E. Shishkin, E. Rumyantsev, E. Nikolaeva, A. Shur, R. Batchko, M. Fejer, K. Gallo, S. Kurimura, K. Terabe *et al.*, Ferroelectrics **304**, 111 (2004).
[17]H. Hu, R. Ricken, and W. Sohler, Opt. Exp. **17**, 24261–24268 (2009).
[18]A. Gruverman, O. Auciello, and H. Tokumoto, Annu. Rev. Mater. Sci. **28**, 101 (1998).
[19]O. Kolosov, A. Gruverman, J. Hatano, K. Takahashi, and H. Tokumoto, Phys. Rev. Lett. **74**, 4309 (1995).
[20]B. J. Rodriguez, A. Gruverman, A. I. Kingon, R. J. Nemanich, and J. S. Cross, J. Appl. Phys. **95**, 1958 (2004).
[21]C. Harnagea, A. Pignolet, M. Alexe, and D. Hesse, Integrated Ferroelectrics **44**, 113–124 (2010).
[22]A. N. Smirnova, S. S. Mushinskiy, I. S. Baturin, I. S. Azanova, D. I. Shevtsov, A. R. Akhmatkhanov, A. V. Ievlev, and V. Y. Shur, Ferroelectrics **441**, 9 (2012).
[23]C. E. Rice and M. Hill, Mater. Res. Bull. **19**, 591 (1984).
[24]W. Hou, W. Hua, Y. Zang, and H. Tan, Electron. Lett. **27**, 755 (1991).
[25]T. Umeki, O. Tadanagai, and M. Asobe, IEEE Photon. Technol. Lett. **23**, 33 (2011).
[26]L. Balobaid, N. C. Carville, M. Manzo, L. Collins, K. Gallo, and B. J. Rodriguez, Appl. Phys. Lett. **103**, 182904 (2013).
[27]D. F. Clark, C. G. Nutt, K. K. Wong, P. J. R. Laybourn, and R. M. De La Rue, J. Appl. Phys. **54**, 6218 (1983).
[28]J. M. White and P. F. Heidrich, Appl. Opt. **15**(1), 151 (1976).
[29]Yu. N. Korkishko and V. A. Fedorov, Tech. Phys. **44**(3), 307–316 (1999).
[30]Y. N. Korkishko and V. A. Fedorov, IEEE J. Sel. Top. Quantum Electron. **2**, 187 (1996).
[31]C. E. Rice, J. Solid State Chem. **64**, 188 (1986).
[32]H. H. Nahm and C. H. Park, Appl. Phys. Lett. **78**, 3812 (2001).
[33]D. Damjanovic, Rep. Prog. Phys. **61**, 1267 (1998).
[34]A. Gruverman and A. Kholkin, Rep. Prog. Phys. **69**, 2443 (2006).
[35]A. L. Kholkin, S. V. Kalinin, A. Roelofs, and A. Gruverman, in *Scanning Probe Microscopy of Electrical and Electromechanical Phenomena at the Nanoscale*, edited by S. V. Kalinin and A. Gruverman (Springer, 2006), Chap. I.6, pp. 173–214.
[36]S. Hong, J. Woo, H. Shin, J. U. Jeon, Y. E. Pak, E. Colla, N. Setter, E. Kim, and K. No, J. Appl. Phys. **89**, 1377 (2001).
[37]S. V. Kalinin and D. A. Bonnell, Phys. Rev. B **65**, 125408 (2002).
[38]C. Durkan, D. P. Chu, P. Migliorato, and M. E. Welland, Appl. Phys. Lett. **76**(3), 366 (2000).
[39]F. Saurenbach and B. D. Terris, Appl. Phys. Lett. **56**, 1703 (1990).
[40]S. Jesse, S. Guo, A. Kumar, B. J. Rodriguez, R. Proksch, and S. V. Kalinin, Nanotechnology **21**, 405703 (2010).
[41]Y. N. Korkishko, V. A. Fedorov, and F. Laurell, IEEE J. Sel. Top. Quantum Electron. **6**, 132 (2000).
[42]A. Loni, R. W. Keys, and R. M. De La Rue, J. Appl. Phys. **67**, 3964 (1990).